Contact Lens and Anterior Eye xxx (xxxx) xxx–xxx

Contents lists available at ScienceDirect

Contact Lens and Anterior Eye

journal homepage: www.elsevier.com/locate/clae

Robust keratoconus detection with Bayesian network classifier for Placido-based corneal indices

Gracia M. Castro-Luna[a,*], Andrei Martínez-Finkelshtein[b,c], Darío Ramos-López[d]

[a] Department of Physiotherapy, Nursing and Medicine, University of Almería, Spain
[b] Department of Mathematics, Baylor University, Texas, USA
[c] Department of Mathematics, University of Almería, Spain
[d] Department of Applied Mathematics, Materials Science and Engineering and Electronic Technology, Rey Juan Carlos University, Madrid, Spain

ARTICLE INFO

Keywords:
Corneal topography
Keratoconus
Placido rings
Keratoconus indices
Bayesian network classifiers
Machine learning

ABSTRACT

Purpose: To evaluate in a sample of normal and keratoconic eyes a simple Bayesian network classifier for keratoconus identification that uses previously developed topographic indices, calculated directly from the digital analysis of the Placido ring images.

Methods: A comparative study was performed on a total of 60 eyes from 60 patients (age 20–60 years) from the Department of keratoconus of INVISION Ophthalmology clinic (Almería, Spain). Patients were divided into two groups depending on their preliminary diagnosis based on the classical topographic criteria: a control group without topographic alteration (30 eyes) and a keratoconus group (30 eyes). The keratoconus group included all grades except grade IV with excessively distorted corneal topography. All cases were examined using the CSO topography system (CSO, Firenze, Italy), and primary corneal Placido-indices were computed, as described in literature. Finally, a classifier was built by fitting a conditional linear Gaussian Bayesian network to the data, using the 5- and 10-fold cross-validation. For comparison, the original data were perturbed with random white noise of different magnitude.

Results: The naïve Bayes classifier showed perfect discrimination ability among normal and keratoconic corneas, with 100% of sensibility and specificity, even in the presence of a very significant noise.

Conclusions: The Bayesian network classifiers are highly accurate and proved a stable screening method to assist ophthalmologists with the detection of keratoconus, even in the presence of noise or incomplete data. This algorithm is easily implemented for any Placido topographic system.

1. Introduction

The most common technology used to measure corneal topography is the Placido disk system [1], based on projecting an illuminated pattern of concentric rings or mires onto the surface of the cornea. The image of these rings is captured and digitized along a fixed number of meridians, which provides several thousand of points in a close-to-concentric pattern. The software of the topographer processes this data to yield elevation, curvature and other parameters using either publicly available (see e.g. [2–6]) or proprietary algorithms. The result is usually represented as color maps, which permits subjective, qualitative analysis of the data; topographic indices aim at providing some objectivity to this analysis. They typically focus on either the entire corneal surface (whole cornea indices) or on a specific subarea (regional indices), and return one or several numerical values characterizing the topography. Since a single index rarely captures the whole complexity of the cornea, composite indices are calculated combining two or more indices.

Many of these indices were developed specifically for early detection and classification of keratoconus (KC), as well as for discrimination between KC and other abnormalities such as contact lens-induced warpage and other forms of irregular astigmatism. Recall that KC is a pathology that produces a cone-shaped deformity in the cornea as a result of degeneration of corneal stroma tissue and subsequent biomechanical alterations [7–13]. This is the cause of a significant increase of the anterior corneal irregularity and a deterioration of the visual quality, since this first surface of the cornea has a very relevant optical function in the eye.

The above mentioned indices take into account the geometry and optical properties of the anterior corneal surface [14–16], although with the widespread use of Scheimpflug cameras more KC characterizations use also pachimetry [17–22]. There have been attempts to complement them with more sophisticated tools such as neural

* Corresponding author.
E-mail address: graciacl@ual.es (G.M. Castro-Luna).

https://doi.org/10.1016/j.clae.2019.12.006
Received 29 June 2019; Received in revised form 3 December 2019; Accepted 6 December 2019

networks [23–25].

In [26,27], a set of indices that measure the irregularity of the anterior corneal surface, computed directly from the image of the Placido disks reflected on the cornea, was put forward. This approach was platform-independent and allowed bypassing the surface or curvature reconstruction step that is currently performed by the software of every commercial Placido topographer. Several basic (or primary) indices were built directly from easy-to-measure parameters of the digitized images of the rings reflected on the cornea. Also, compound metrics were proposed (such as the generalized linear model or the classification trees) by combining some of the primary indices to improve their efficiency.

One of the conclusions of [26,27] was that the primary indices allow to discriminate, with excellent accuracy, between normal eyes and eyes with keratoconic corneas. As expected, combined indices were even more efficient. Nevertheless, both the generalized linear model and the classification trees have a natural intrinsic weakness: they deal poorly with noisy or incomplete data, something that occurs very often in clinical practice. The goal of this work is to replace these metrics with a new combined index that based on the values of the primary indices from [26,27] calculated from possibly noisy data, could yield no less accurate but more robust results. This was made possible by considerable recent advances experiences in the fields of computational statistics, artificial intelligence and machine learning.

Bayesian networks (BNs) are a flexible probabilistic tool that has been successfully used for solving complex problems, including inference, classification and regression [28,29]. They consist of a qualitative and a quantitative component. The former is a directed acyclic graph (DAG), which represents the dependencies between the variables; the latter is a set of conditional probability distributions, from which the joint probability distribution can be recovered. The network structure (the DAG) can be learned automatically or fixed manually using expert knowledge about the problem. A typical DAG structure is the naïve Bayes (NB) model, which has been extensively used in classification problems due to its good results in terms of accuracy [30–33]. In a NB classifier, there is a *class variable* which is the only parent of the rest of variables (*explanatory variables*) in the DAG. This model works on Bayes theorem of probability to predict the class data set assuming conditional independence among predictors, given the class. Naïve Bayes model is fast, easy to build, requires only a small number of training data to estimate its parameters, and is known to outperform even some highly sophisticated classification methods [29].

In this paper, the topographic indices from [26,27] were used to build a BN, or more precisely, a naïve Bayes classifier, and to evaluate its usefulness for the detection of corneal topographic keratoconus, comparing its accuracy and robustness to faulty measurements with the compound indices form [27], using for that both synthetic and real patients data.

2. Patients and methods

2.1. Patients

This study uses data of 60 eyes from 60 patients aged 20–60 years (mean 33.86 ± 11.46 years) from the Department of Keratoconus of INVISION Ophthalmology clinic (Almería, Spain). They were divided into two groups according to whether they were diagnosed with KC or not: a control group (30 eyes) and a KC group (30 eyes). Inclusion in the KC group was based on the criteria established for the diagnosis of this corneal pathology and the absence of ocular surgical history that could have modified it. The diagnostic criteria were: asymmetric bow tie in the topographic image and at least one sign of keratoconus in the examination with the slit lamp, such as stromal thinning, conical protrusion of the cornea at the apex, Fleischer ring, Vogt striae or anterior stromal scar. For contact lens wearers it was recommended to stop wearing them for two weeks for soft contact lenses and four weeks for gas permeable rigid contact lenses. The exclusion criteria were the existence of any ocular pathology and the presence of advanced KC (grade 4 according to the Alió-Shabayek classification system [14]). In cases of unilateral keratoconus, the affected eye was always included in the study. For patients with bilateral keratoconus, only one eye was randomly selected for the study.

The control group included eyes with normal corneal topography with no signs of irregularity according to the indices mentioned above, without ocular pathology or previous ocular surgery. In this control group, only one eye from each patient was selected for inclusion in the study. All patients were informed about the objectives of the study, voluntarily agreed to their participation and signed an informed consent document in accordance with the Declaration of Helsinki.

For all patients, corneal topographic analysis was carried out with CSO topography system (CSO, Firenze, Italy). This topographer analyses a total of 6144 corneal points of a corneal area delimited by a circular ring defined by an interior radius and an exterior radius of 10 mm with respect to the corneal vertex. The software of this system, EyeTop2005 (CSO, Florence, Italy), allows access to the raw data and their export to an ASCII file, necessary for the calculation of the primary corneal indices described next.

2.2. Corneal indices

In [26], a methodology for building metrics based directly on the image captured by the digital camera of the Placido-based topographers was put forward, and a set of corneal indices was introduced as an additional tool for keratoconus (and in general, cornea irregularity) detection and classification. Later their performance was analyzed in [27]. Some of these indices are described next for the reader's convenience.

At the beginning, the digitized points captured by the camera of a Placido disk corneal topographer are grouped in mires; in defining the indices, only data from complete rings are used, limiting the number of rings to the maximum of $N \leq 15$. For each mire, numbered by the integer value $1 \leq k \leq N$ starting from the innermost one, the best-fit circle was calculated, namely its radius, denoted by $AR(k)$ (from "average ring radius" of the kth ring), and the position of its center C_k, in Cartesian coordinates. In what follows, only the radii $AR(1)$ and $AR(4)$ of the 1st and 4th mires are used. Additional four primary indices were calculated, the first three labeled as PI_n (from "Placido Irregularity indices"):

1 The diameter of the set of centers C_k (normalized by the total number of rings N),

$$\mathrm{PI}_1 = \frac{1}{N}\max_{1\leq n,m\leq N}\|C_n - C_m\|,$$

where $\|\cdot\|$ is the standard Euclidean norm in $\mathbb{R}^2$. PI_1 represents the maximum distance between the centers of individual mires. Thus, large values of PI_1 correlate with substantial asymmetry and off-centering of the rings.

2 The total drift or deviation in the consecutive centers,

$$\mathrm{PI}_2 = \frac{1}{N-1}\sum_{1\leq n\leq N-1}\|C_{n+1} - C_n\|.$$

PI_2 represents the length of the path connecting the consecutive centers of individual mires. Large values of PI_2 mean an important drift in the centers' positions, and this index is therefore another measure of asymmetry.

3 For the third index the data from mires are fit with an ellipse, and the dispersion of the values of the axis ratios r_k (see [26,27] for details) is measured, defining

$$\mathrm{PI}_3 = \sqrt{\frac{1}{N}\sum_{1\leq k\leq N}(r_k - \bar{r})^2}, \quad \text{where} \quad \bar{r} = \frac{1}{N}\sum_{1\leq k\leq N} r_k.$$

In other words, PI_3 measures the variability in the eccentricity of the mires approximated by ellipses.

4 *SL* stands for the absolute value of the slope of the standard linear regression of the coordinates of the centers C_k, so that high values of *SL* correspond to a vertical alignment of the centers. *SL* measures the orientation of the path connecting the centers, so that it has high values when the centers' drift is almost vertical and low values when it is horizontal.

Additionally, a combined metric called GLPI (from Generalized Linear Placido Irregularity index) was introduced in [26] and improved later in [27]. It uses the indices PI_1, PI_3, $AR(4)$ and *SL* as input, and takes continuous values between 0 and 100 (0% corresponding to a totally normal, and 100%, to a totally altered cornea), see [27] for details.

2.3. Bayesian networks

A graph is a set of vertices or nodes and a set of edges or arcs connecting them. A directed graph is one in which all the arcs have a direction (i.e., they point from one node to another). A directed graph is acyclic (or in short, DAG) when it does not contain loops or closed paths (cycles), as the nodes are traversed following the direction of the edges, see e.g. Fig. 1. A Bayesian network is a compact representation of the joint probability distribution over a set of variables $\boldsymbol{X} = \{X_1, ..., X_n\}$ whose independence relations are encoded by the structure of an underlying DAG [34]. Formally, a BN is defined as a pair (G, P), where G is a DAG and P is a set of conditional probability distributions (CPDs). G is composed of nodes that represent random variables $(\boldsymbol{X})$, and links between pairs of nodes representing statistical dependence. Each node X_i has an associated probability distribution $p(X_i \mid \mathrm{Pa}(X_i))$, where $\mathrm{Pa}(X_i)$ denotes the parents of X_i in the DAG G. The joint probability distribution over all the variables in the network can be recovered as the product of the CPDs attached to each node (chain rule):

$$p(X_1, ..., X_n) = \prod_{i=1}^{n} p(X_i \mid \mathrm{Pa}(X_i)), \quad \text{for } X_i \in \Omega_i, \quad i = 1, ..., n,$$

where Ω_i represents the domain or set of all possible values of the variable X_i. In a naïve Bayes (NB) classifier, the DAG G consist of $n - 1$ links, pointing from the class variable Y to each of the explanatory variables X_i. In other words, it assumes independence among predictors. In this study, NB classifiers with a discrete class variable Y, taking values in a finite set $\{y_1, \ldots, y_m\}$ were considered. The goal of such a classifier is, given the values of explanatory variables $\boldsymbol{X}$ (not necessarily all of them), to determine the probability of the features occurring in each class $\{Y = y_j\}$, and to return the most likely one:

$$\mathrm{argmax}_j \, p(Y = y_j \mid \boldsymbol{X}).$$

This is done using Bayesian probability theorem, according to which

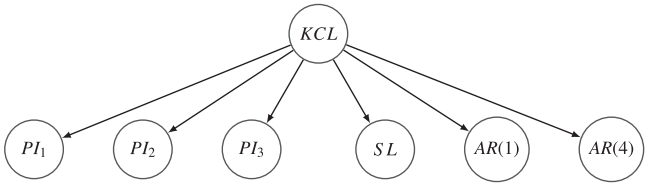

Fig. 1. Naïve Bayes classifier built from Placido-based indices explained in Section 2.2. PI_1 represents the maximum distance between the centers of individual mires; PI_2 is the length of the path connecting the consecutive centers of individual mires; PI_3 is a measure of variability in the eccentricity of the mires, approximated by ellipses; SL measures the orientation of the path connecting the centers. Finally, $AR(1)$ and $AR(4)$ are the radii of the circles fitting the images of the first and fourth mire, respectively.

$$\text{posterior} = \frac{\text{prior} \times \text{likelihood}}{\text{evidence}}.$$

In other words, the posterior probability distribution over the class variable Y is calculated by performing *probabilistic inference* (also called *belief update*) as follows:

$$p(Y = y_j \mid \boldsymbol{X}) = \frac{p(Y = y_j) p(\boldsymbol{X} \mid Y = y_j)}{p(\boldsymbol{X})} = \frac{p(Y = y_j) \prod_{i=1}^{n} p(X_i \mid Y = y_j)}{\sum_{j=1}^{m} p(Y = y_j) p(\boldsymbol{X} \mid Y = y_j)}, \quad j = 1, ..., m.$$

The probability ratio above can be estimated by generating a large sample from the Bayesian network and using evidence weighting [35].

The NB model can be validated employing the k-fold cross-validation technique [36], obtaining a measure of error in each fold. This technique randomly splits the complete dataset into k subsets, using $k - 1$ of them for learning (train set) and the other for validation (test set). The performance in the classification task is evaluated by computing, in every fold, the accuracy, precision, recall and F_1 score of the computed model over its test set.

The programming language R, version 3.5.1, was the computational tool used. In particular, the BN were built using the R package `bnlearn` [37], while the primary corneal Placido-based indices were calculated by means of the R package `rPACI` [38].

3. Results

3.1. Optometric data

The study included a total of 60 patients, divided into two groups regardless gender: 30 eyes with keratoconus (keratoconus group) and 30 normal eyes (control group). Table 1 shows a summary of the visual, refractive, topographic and aberrometric data of the cornea in the two eye groups analyzed in the present study, keratoconus and control group.

As expected, statistically significant differences were found between the groups in uncorrected distance visual acuity (unpaired Student t test, $p = 0.04$) and corrected (Mann-Whitney test, $p < 0.01$), with the worst vision for the keratoconus group. The eyes of this group also presented a significantly larger refractive cylinder component (Mann-Whitney test, $p < 0.01$) and, consequently, a significantly larger topographic astigmatism (Mann-Whitney test, $p < 0.01$). Keratoconus corneas presented significantly more negative corneal asphericity (oblique or parabolic shape). With respect to high order corneal aberrations, greater amounts of spherical and coma aberrations (unpaired Student t test, $p < 0.01$) occurred in keratoconus corneas, with no significant differences between groups in the level of primary spherical aberrations (Mann–Whitney, $p = 0.30$), see Table 1.

3.2. Corneal indices

Table 2 summarizes the results, both for the control and keratoconus groups. As shown, all indices were significantly higher in the KC group. In the specific case of PI_2, the range of values obtained for both groups were significantly different and almost did not overlap.

The average mean radius of the first ring, $AR(1)$, was significantly higher in the keratoconus group (mean 57.95, SD 27.49) compared to the control group (mean 21.12, SD 10.38); unpaired t Student test rendering $p < 0.01$.

For the combined index GLPI, a statistically significant difference was found between the KC group (mean 95.97; SD 12.03) and the control group (mean 4.39; SD 10.53), with Mann-Whitney test giving $p < 0.01$. Again, the indices included in the linear model as defined in [27] were *SL*, PI_1, PI_3 and $AR(4)$.

Table 1
Summary of the visual, refractive, corneal topographic, and corneal aberrometric data (mean and range) of the two groups of eyes analyzed in the current study, Keratoconus and Control groups. P-values for the comparison among groups for each clinical parameter are also given. Abbreviations: SD, standard deviation; D, diopters; UDVA, uncorrected distance visual acuity; CDVA, corrected distance visual acuity; K1, corneal dioptric power in the flattest meridian for the 3 mm central zone; K2, corneal dioptric power in the steepest meridian for the 3 mm central zone; KM, mean corneal power in the 3 mm zone; AST3, corneal astigmatism for the 3-mm central zone; AST6, corneal astigmatism for the 6-mm central zone; Q45, mean asphericity for a corneal area of 4.5-mm diameter; Q8, mean asphericity for a corneal area of 8-mm diameter; RMS, root mean square.

Clinical parameters	KC group mean (range)	Control group mean (range)	*p*-value
Visual parameters			
LogMAR UDVA	0.57 (0.01 to 1.30)	0.30 (−0.18 to 1.30)	0.04
LogMAR CDVA	0.17 (0.00 to 0.82)	0.03 (−0.18 to 0.36)	< 0.01
Refractive parameters			
Sphere (D)	−1.60 (−11.00 to +2.25)	−1.92 (−14.00 to +2.75)	0.86
Cylinder (D)	−3.01 (−6.75 to −0.50)	−1.03 (−4.50 to 0.00)	< 0.01
Topographic parameters			
K 1 (D)	45.13 (41.22 to 50.41)	42.82 (40.07 to 45.53)	< 0.01
K 2 (D)	48.72 (42.48 to 57.16)	44.04 (41.30 to 46.62)	< 0.01
KM (D)	46.92 (41.90 to 53.71)	43.44 (41.00 to 46.17)	< 0.01
AST 3 (D)	4.00 (0.68 to 11.04)	1.22 (0.31 to 4.12)	< 0.01
AST 6 (D)	3.40 (0.67 to 9.71)	1.22 (0.23 to 3.94)	< 0.01
Q 45	−0.79 (−2.56 to +0.60)	+0.31 (−0.44 to +1.48)	< 0.01
Q 8	−0.32 (−1.24 to +0.64)	+0.23 (−0.51 to +1.12)	< 0.01
Corneal aberrometry			
Primary spherical aber. (μm)	−0.20 (−0.51 to +0.14)	−0.12 (−0.40 to +0.33)	0.30
Primary coma RMS (μm)	1.64 (0.57 to 3.99)	0.27 (0.06 to 0.55)	< 0.01
Higher order residual RMS (μm)	0.86 (0.20 to 1.63)	0.23 (0.10 to 0.44)	< 0.01
Spherical-like RMS (μm)	0.53 (0.14 to 1.38)	0.24 (0.09 to 0.45)	< 0.01
Coma-like RMS (μm)	1.80 (0.59 to 4.05)	0.34 (0.13 to 0.67)	< 0.01

Table 2
Summary of the values obtained for the primary corneal indices PI_1-PI_3 in the control and keratoconus groups for the current study. *p*-values for the comparison among groups for each primary corneal index (PI_j) corresponding to Mann-Whitney test are also given. Abbreviation: SD, standard deviation.

Primary indices	KC group		Control group		*p*-value
	Mean (SD)	Range	Mean (SD)	Range	
PI_1	129.67 (31.92)	40–150	19.16 (15.41)	1–58	< 0.01
PI_2	121.47 (33.60)	52–150	24.84 (13.32)	1.00–53.00	< 0.01
PI_3	92.92 (50.87)	8–150	22.68 (18.39)	1–68	< 0.01

3.3. NB model

A naïve Bayes classifier was built, by fitting a *conditional linear Gaussian* (CLG) Bayesian network to the data. In other words, the class variable, called **KCL** (from "Keratoconus Likelihood"), takes the values 0 (= "normal eye") and 1 = (keratoconus) with a binomial distribution, while the explanatory variables (primary indices *SL*, PI_1, PI_2, PI_3, *AR*(1) and *AR*(4)) follow a conditional linear Gaussian distribution (i.e., a normal distribution for each value of the parent KCL). The structure of the network is depicted in Fig. 1. Although this choice assumes independence among predictors, which is not easy to justify, the dependence turned out to be sufficiently weak to ensure excellent results without recurring to more complex network topology.

The conditional distributions obtained for each variable using the methodology explained in Section 2.3 (with assumption $p(\mathrm{KCL}=0) = p(\mathrm{KCL}=1) = 0.5$) are indicated in Table 3, where the notation

$$X|\,\mathrm{KCL} = v \sim N(\mu, \sigma)$$

expresses that the probability distribution for the variable *X*, given that its parent "KCL" takes the value *v*, is a normal distribution with mean μ and standard deviation σ.

This model was validated using *k*-fold cross-validation (with randomly chosen folds), with $k = 5$ and $k = 10$. The results for the NB model were identical in both cases: the values obtained of *accuracy* (ratio of correctly predicted observations to the total observations), *precision* (ratio of correctly predicted positive observations to the total predicted positive observations), *recall* or sensitivity (ratio of correctly predicted positive observations to all observations in the class "1") and *F1-score* (harmonic mean of precision and recall) were all 1.0, which means a perfect classification in both groups, on every fold.

Table 3
Parameters μ, σ of the normal distribution $N(\mu, \sigma)$ corresponding to the conditional probability of the explanatory variables.

Expl. var. *X*	$X\|\,\mathrm{KCL}=1 \sim N(\mu,\sigma)$	$X\|\,\mathrm{KCL}=0 \sim N(\mu,\sigma)$
PI_1	$\mu = 131.2$, $\sigma = 35$	$\mu = 19.5$, $\sigma = 11.7$
PI_2	$\mu = 125$, $\sigma = 34.4$	$\mu = 29.3$, $\sigma = 9.2$
PI_3	$\mu = 93.5$, $\sigma = 52.4$	$\mu = 35.9$, $\sigma = 14.7$
SL	$\mu = 115$, $\sigma = 43.9$	$\mu = 21.6$, $\sigma = 14.8$
AR(1)	$\mu = 96.1$, $\sigma = 28.5$	$\mu = 53.4$, $\sigma = 9.2$
AR(4)	$\mu = 58.9$, $\sigma = 17.5$	$\mu = 31.3$, $\sigma = 5.4$

For comparison purposes, same analysis was carried out for the compound index GLPI as defined in [27]. In fact, two variants were tested: using the original definition from [27] that involves only variables (PI_1, PI_3, *SL* and *AR*(4)), and extended GLPI involving now the same variables as in the NB model (that is, $PI_1 - PI_3$, *SL*, *AR*(1) and *AR*(4)). The original GLPI index yielded accuracy values of 0.983, while the extended GLPI index gave an accuracy of 0.967. This decrease can be explained by the introduction of linearly correlated explanatory variables in the model; the generalized linear model is more sensitive to this issue than the NB. The results were consistent with those published previously in [27], where the accuracy of GLPI was reported to be of 0.94 − 0.95 (depending on the type of cross-validation used). Notice that the precision for both indices was 1.0, meaning that every eye classified as KC was indeed a keratoconus (no false positives). In other words, GLPI have good specificity but worse sensitivity.

The results of the experiments are summarized in Table 4 (using 10-fold cross-validation) and Table 5 (using 5-fold cross-validation).

In order to test the sensitivity of the classifiers to measurement errors, another complementary experiment was carried out, in which random measurement errors were simulated. Gaussian white noise of a

Table 4
Mean values of the different metrics using 10-fold cross-validation.

10-fold CV	NB model	Original GLPI	Extended GLPI
Accuracy	1.000	0.983	0.967
Precision	1.000	1.000	1.000
Recall	1.000	0.967	0.942
*F*1-Score	1.000	0.980	0.966

Table 5
Mean values of the different metrics using 5-fold cross-validation.

5-fold CV	NB model	Original GLPI	Extended GLPI
Accuracy	1.000	0.983	0.967
Precision	1.000	1.000	1.000
Recall	1.000	0.95	0.928
*F*1-Score	1.000	0.971	0.960

specific magnitude (m) was added to the coordinates of the nodes (points on the images of the Placido rings), so that the coordinates of the nodes were modified according to the expressions

$$x_j \longleftarrow x_j + m\,\beta_j, \quad y_j \longleftarrow y_j + m\,\eta_j,$$

where β_j, η_j are independent random variables with distribution $N(0, 1)$, and m is the noise amplitude. The effect of these perturbations on the original data can be seen in Fig. 2 for different values of m: 0 (no perturbation), 0.02, 0.04 and 0.08. This is obviously the worst case scenario: usually central region is less affected by random noise than the periphery.

The primary Placido indices were calculated using these artificially perturbed data. The distributions of individual Placido indices and their pairs are depicted in Fig. 3, for several noise levels. These plots illustrate the ability of every single index and every pair of indices to discriminate between keratoconic and normal eyes. They also show the change in their distributions when the data are perturbed, and how their values tend to be more overlapping between the two groups after adding noise. However, the plots also indicate that the Placido indices maintain their discriminating ability, even in the presence of moderately high noise.

The newly calculated primary corneal indices were fed to the different classifiers (the NB model, GLPI and extended GLPI) in order to re-evaluate their accuracy in presence of noise. For the sake of brevity, only the results of the 10-fold cross-validation (Table 6) are presented.

These results show that, even though the three models (and the primary indices they are based on) are rather robust to measurement errors, the NB model still performs perfectly (accuracy of 1.000, which means a perfect classification in each group) in the presence of noise (for $m = 0.02$ and 0.04). In the presence of a strong noise component ($m = 0.06$), the accuracy of the NB model decreases, but still outperforms the other two models.

4. Discussion and summary

In the advanced stages of keratoconus, clinical diagnosis is not a

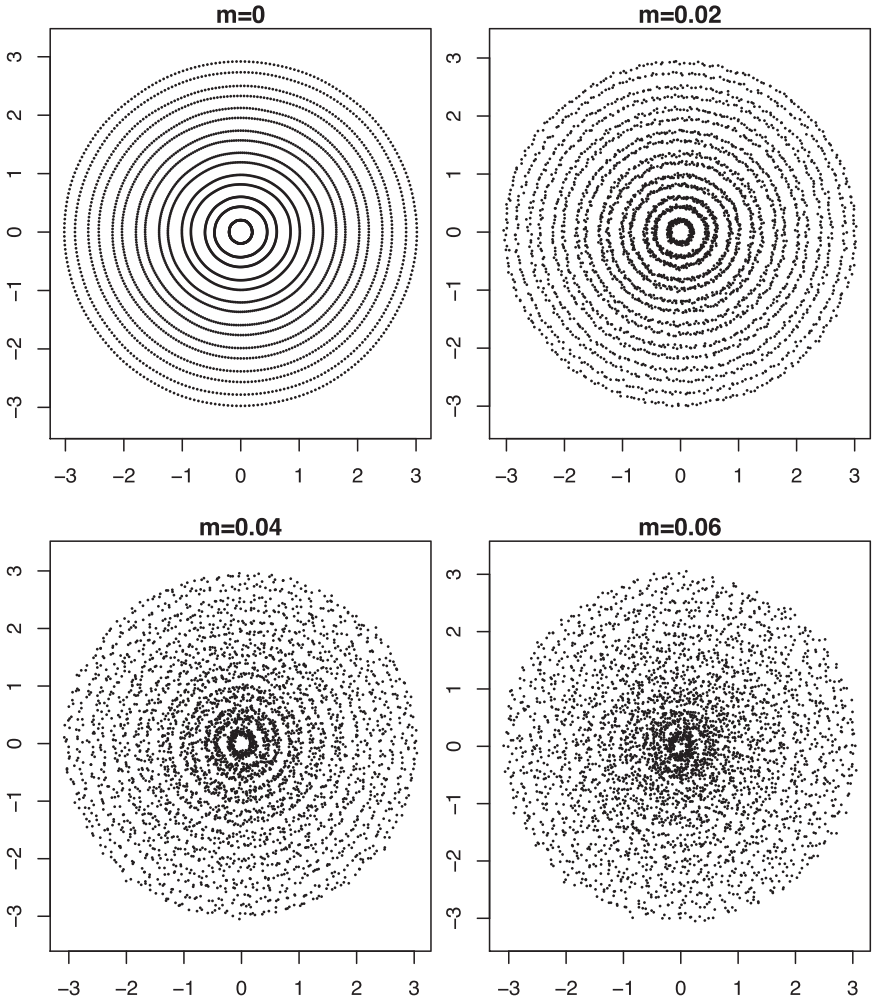

Fig. 2. Raw data after introducing perturbations of different amplitudes.

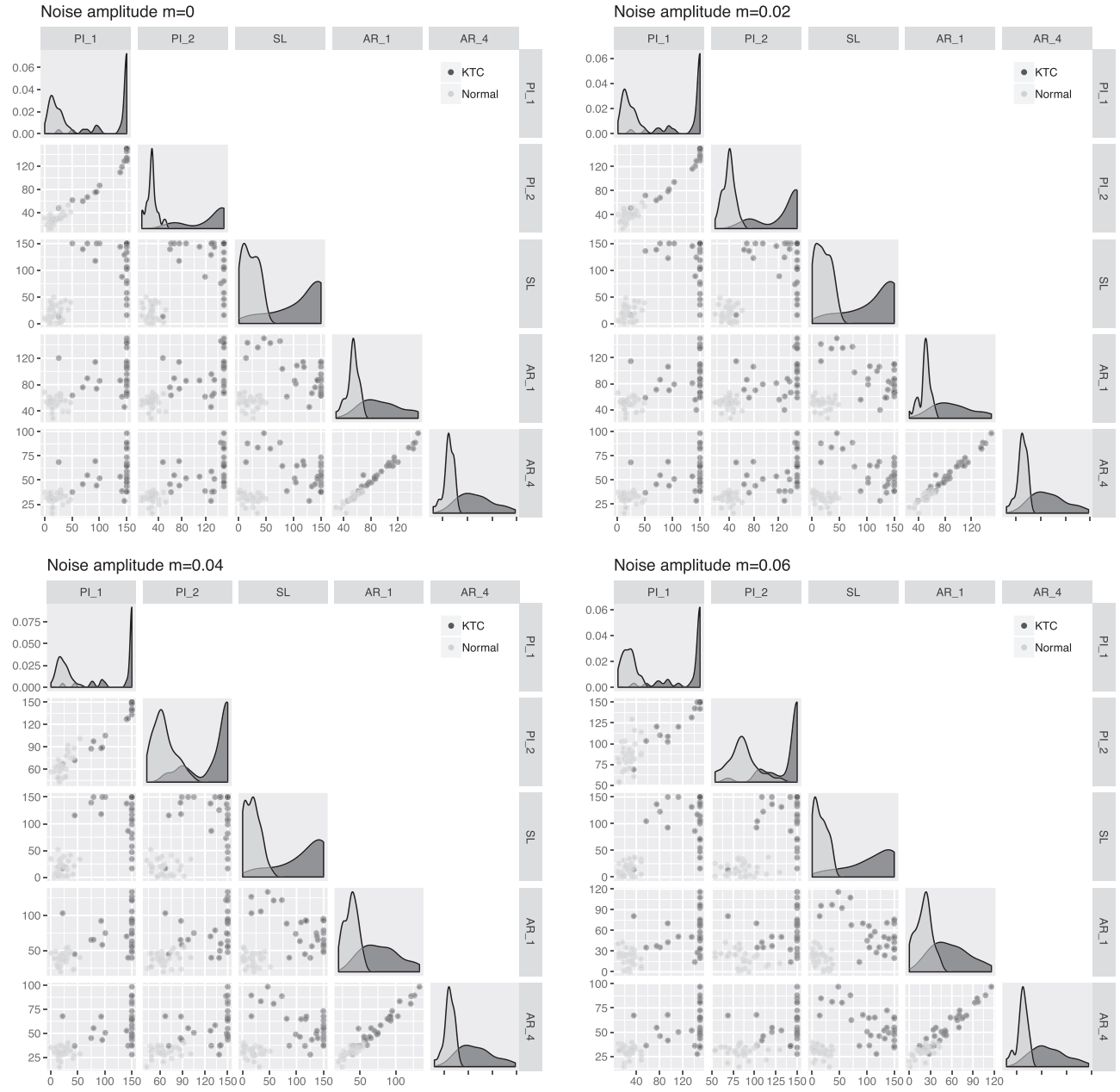

Fig. 3. Scatter plots of some of the primary Placido indices calculated using the artificially perturbed data. These plots illustrate the change in the distribution of these indices between the two groups when the noise level in the data varies, becoming their values more overlapping, but without loosing the discrimination ability.

Table 6
Accuracy of the compared metrics in presence of Gaussian noise of different amplitudes, using 10-fold cross-validation.

Noise amplitude m	NB model	Original GLPI	Extended GLPI
0.00	1.000	0.983	0.967
0.02	1.000	0.983	0.967
0.04	1.000	0.967	0.967
0.06	1.000	0.967	0.933

major problem due to biomicroscopic, retinoscopic and pachymetric signs [9]. However, in the preclinical stages of the disease, it is a challenge for the ophthalmologist in the absence of obvious clinical signs, being extremely important due to the contraindication in these patients of performing corneal refractive surgery, in addition to being able to treat KC early and eventually prevent its progression. But in the early stages of the disease, the diagnosis of keratoconus is primarily based on corneal topography. The analysis of corneal topography data with increasingly sophisticated software attempts to help the clinician to detect and diagnose these keratoconic alterations. A set of simple and apparently efficient indices for Placido-based corneal topographers (pervasive and still dominant in the clinical practice) was proposed in [26] and evaluated in [27]. There, the two-stage approach was implemented: originally defined primary corneal indices, calculated from the images of the reflection of the rings on the corneal surface, were combined into different type of classifiers, considerably increasing their performance. In particular, classification trees and a generalized linear model (GLPI) were used.

Since then, computational statistics, artificial intelligence and machine learning have experienced a major breakthrough. The goal of this work was to address one of the weaknesses of the combined indices from [26,27], namely their sensitivity to the data quality. Unfortunately, noisy data are common in the clinical practice. Naïve Bayes classifiers, as the one developed in this work, have a number of

advantages with respect to the classical approach. As the study showed, they are more robust to quality degradation of the input data, without loosing their discrimination ability.

A comparison of the new NB classifier with the combined indices from [26,27] was carried out using an independent database of 60 patients, such as described in Section 2.1. Also, the original data was perturbed with random noise of diverse amplitude. In all cases, the NB showed an excellent discriminatory performance. The values obtained of accuracy, precision, recall and *F*1-score were all 1.0, which means a perfect classification in both groups (KC and normal cornea), on every fold. The results achieved with the original indices were consistent with those published in [26,27].

In conclusion, the use of naïve Bayes classifiers feeding from the original corneal indices (and valid for use with any Placido disc-based topographer) provides adequate criteria for the topographic diagnosis of keratoconus. They inherit all the advantages of the primary indices described in [26,27], providing an additional robustness to noisy or incomplete data, are not computationally intense and are platform-independent, being easily implemented for any Placido topographic system that represent the vast majority of surveying devices available in clinical practice.

Conflict of interest

All three authors declare that they have no conflict of interest, no funding or grants or equipment provided for the project from any source, no financial benefits to the authors. The software for the calculation of corneal indices is an intellectual property copyright of the authors and is currently used for experimental purposes only.

Ethical approval: All procedures performed in studies involving human participants were in accordance with the ethical standards of the institutional and national research committee and with the 1964 Helsinki declaration and its later amendments or comparable ethical standards.

Informed consent: Informed consent was obtained from all individual participants included in the study.

Acknowledgments

This research was partially supported by Junta de Andalucía (grant PIN-0530-2017). Research of A.M.-F. and D.R.-L. was also supported in part by the Spanish Government – European Regional Development Fund (grant MTM2017-89941-P), Junta de Andalucía (research group FQM-229), and by the University of Almería (Campus de Excelencia Internacional del Mar CEIMAR). A.M.-F. acknowledges an additional support from Instituto Interuniversitario Carlos I de Física Teórica y Computacional, while D.R.-L. thanks the support from CDTIME (University of Almería).

References

[1] Y. Mejía-Barbosa, D. Malacara-Hernández, A review of methods for measuring corneal topography, Optomet Vision Sci 78 (4) (2001) 240–253.
[2] P.P. van Saarlos, I.J. Constable, Improved method for calculation of corneal topography for any photokeratoscope geometry, Optomet Vision Sci 68 (12) (1991) 960–965.
[3] S.A. Klein, A corneal topography algorithm that produces continuous curvature, Optomet Vision Sci 69 (11) (1992) 829–834.
[4] M.A. Halstead, B. Barsky, S.A. Klein, R.B. Mandell, A spline surface algorithm for reconstruction of corneal topography from a videokeratographic reflection pattern, Optomet Vision Sci 72 (11) (1995) 821–827.
[5] S.A. Klein, Corneal topography reconstruction algorithm that avoids the skew ray ambiguity and the skew ray error, Optomet Vision Sci 74 (1997) 945–962.
[6] V.A.D.P. Sicam, R.G.L. Van der Heijde, Topographer reconstruction of the non-rotation-symmetric anterior corneal surface features, Optom Vis Sci 83 (12) (2006) 910–918, https://doi.org/10.1097/01.opx.0000250018.82043.a6.
[7] Y.S. Rabinowitz, Keratoconus, Surv Ophthalmol 42 (1998) 297–319.
[8] D. Piñero, J.L. Alió, R.I. Barraquer, R. Michael, R. Jiménez, Corneal biomechanics, refraction, and corneal aberrometry in keratoconus: an integrated study, Invest Ophthalmol Vis Sci 51 (2010) 1948–1955.
[9] S. Shah, M. Laiquzzaman, R. Bhojwani, S. Mantry, I. Cunliffe, Assessment of the biomechanical properties of the cornea with the Ocular Response Analyzer in normal and keratoconic eyes, Invest Ophthalmol Vis Sci 48 (2007) 3026–3031.
[10] K. Meek, S. Tuft, Y. Huang, P. Gill, S. Hayes, R. Newton, A. Bron, Changes in collagen orientation and distribution in keratoconus corneas, Invest Ophthalmol Vis Sci 46 (6) (2005) 1948–1956, https://doi.org/10.1167/iovs.04-1253.
[11] A. Daxer, P. Fratzl, Collagen fibril orientation in the human corneal stroma and its implication in keratoconus, Invest Ophthalmol Vis Sci 38 (1) (1997) 121–129.
[12] A. Daxer, P. Fratzl, Erratum: Collagen fibril orientation in the human corneal stroma and its implication in keratoconus (investigate ophthalmology and visual science (1997) 38 (121-129)), Invest Ophthalmol Vis Sci 38 (7) (1997).
[13] M. Smolek, W. Beekhuis, Collagen fibril orientation in the human corneal stroma and its implications in keratoconus, Invest Ophthalmol Vis Sci 38 (7) (1997) 1289–1290.
[14] J.L. Alió, M.H. Shabayek, Corneal higher order aberrations: a method to grade keratoconus, J Refract Surg 22 (2006) 539–545.
[15] M. Gobbe, M. Guillon, Corneal wavefront aberration measurements to detect keratoconus patients, Cont Lens Anterior Eye 28 (2) (2005) 57–66, https://doi.org/10.1016/j.clae.2004.12.001.
[16] S. Barbero, S. Marcos, J. Merayo-Lloves, E. Moreno-Barriuso, Validation of the estimation of corneal aberrations from videokeratography in keratoconus, J Refract Surg 18 (2002) 263–270.
[17] R. Ambrósio, B. Lopes, F. Faria-Correia, M. Salomão, J. Bühren, C. Roberts, A. Elsheikh, R. Vinciguerra, P. Vinciguerra, Integration of Scheimpflug-based corneal tomography and biomechanical assessments for enhancing ectasia detection, J Refract Surg 33 (7) (2017) 434–443, https://doi.org/10.3928/1081597X-20170426-02.
[18] R. Shetty, H. Rao, P. Khamar, K. Sainani, K. Vunnava, C. Jayadev, L. Kaweri, Keratoconus screening indices and their diagnostic ability to distinguish normal from ectatic corneas, Am J Ophthalmol 181 (2017) 140–148, https://doi.org/10.1016/j.ajo.2017.06.031.
[19] J. Steinberg, N. Amirabadi, A. Frings, J. Mehlan, T. Katz, S. Linke, Keratoconus screening with dynamic biomechanical in vivo Scheimpflug analyses: A proof-of-concept study, J Refract Surg 33 (11) (2017) 773–778, https://doi.org/10.3928/1081597X-20170807-02.
[20] A. Martínez-Abad, D. Piñero, New perspectives on the detection and progression of keratoconus, J Cataract Refract Surg 43 (9) (2017) 1213–1227, https://doi.org/10.1016/j.jcrs.2017.07.021.
[21] S. Huseynli, J. Salgado-Borges, J.L. Alió, Comparative evaluation of Scheimpflug tomography parameters between thin non-keratoconic, subclinical keratoconic, and mild keratoconic corneas, Eur J Ophthalmol 28 (5) (2018) 521–534, https://doi.org/10.1177/1120672118760146.
[22] D. Piñero, J. Alió, A. Alesón, M. Escaf, M. Miranda, Pentacam posterior and anterior corneal aberrations in normal and keratoconic eyes, Clin Exp Optomet 92 (3) (2009) 297–303.
[23] L.A. Carvalho, Preliminary results of neural networks and Zernike polynomials for classification of videokeratography maps, Optomet Vision Sci 82 (2) (2005) 151–158.
[24] P.A. Accardo, S. Pensiero, Neural network-based system for early keratoconus detection from corneal topography, J Biomed Inform 35 (2002) 151–159.
[25] I. Issarti, A. Consejo, M. Jiménez-García, S. Hershko, C. Koppen, J. Rozema, Computer aided diagnosis for suspect keratoconus detection, Comput Biol Med 109 (2019) 33–42, https://doi.org/10.1016/j.compbiomed.2019.04.024.
[26] D. Ramos-López, A. Martínez-Finkelshtein, G.M. Castro-Luna, D. Piñero, J.L. Alió, Placido-based indices of corneal irregularity, Optomet Vision Sci 88 (10) (2011) 1220–1231.
[27] D. Ramos-López, A. Martínez-Finkelshtein, G.M. Castro-Luna, N. Burgera-Giménez, A. Vega-Estrada, D. Piñero, J.L. Alió, Screening subclinical keratoconus with Placido-based corneal indices, Optomet Vision Sci 90 (4) (2013) 335–343.
[28] P. Larrañaga, S. Moral, Probabilistic graphical models in artificial intelligence, Appl Soft Comput 11 (2011) 1511–1528.
[29] N. Friedman, D. Geiger, M. Goldszmidt, Bayesian network classifiers, Mach Learn 29 (1997) 131–163.
[30] G.N. Bressan, V.A. Oliveira, E.R. Hruschka, M.C. Nicoletti, Using Bayesian networks with rule extraction to infer risk of weed infestation in a corn-crop, Eng Appl Artif Intel 22 (2009) 579–592.
[31] M. Markus, I. Hejazi, P. Bajcsy, O. Giustolisi, A. Savic, Prediction of weekly nitrate-N fluctuations in a small agricultural watershed in Illinois, J Hydroinformat 12.3 (2010) 251–261.
[32] N. Fytilis, D.M. Rizzo, Coupling self-organizing maps with a Naïve Bayesian classifier: Stream classification studies using multiple assessment data, Water Resour Res 49 (2013) 7747–7762.
[33] A.D. Maldonado, L. Uusitalo, A. Tucker, T. Blenckner, P.A. Aguilera, A. Salmerón, Prediction of a complex system with few data: Evaluation of the effect of model structure and amount of data with dynamic bayesian network models, Environ Model Softw 118 (2019) 281–297.
[34] J. Pearl, Probabilistic reasoning in intelligent systems, Morgan-Kaufmann, 1988.
[35] R. Fung, K.C. Chang, Weighting and integrating evidence for stochastic simulation in Bayesian networks, Uncertainty Artif Intel 5 (1990) 209–220.
[36] M. Stone, Cross-validatory choice and assessment of statistical predictions, J Royal Stat Soci. Series B (Methodological) 36 (2) (1974) 111–147.
[37] M. Scutari, Learning bayesian networks with the bnlearn R package, J Stat Softw 35 (3) (2010) 1–22.
[38] D. Ramos-López, A.D. Maldonado, Placido analysis of corneal irregularity, R package version 0.1.1, Tech. rep. University of Almeria, 2019, https://CRAN.R-project.org/package=rPACI.